

Activity and quiescence in galaxies at redshifts $1.4 < z < 3.5$. The role of the starburst temperature. (Research Note)

M. Contini^{1,2}¹ Dipartimento di Fisica e Astronomia, University of Padova, Vicolo dell'Osservatorio 2. I-35133 Padova, Italy² School of Physics and Astronomy, Tel Aviv University, Tel Aviv 69978, Israel

Received

ABSTRACT

We investigate ‘activity’ and ‘quiescence’ in galaxies at relatively high redshifts by modelling the line (and continuum) spectra of each object. The models account consistently for photoionization and shocks. We claim that the starburst effective temperature, the flux from an AGN, and the shock velocity are critical to activity. The results confirm that two sample galaxies show intense starburst activity with temperatures reaching $T_* = 2 \cdot 10^5 \text{ K}$ and shock velocities $V_s > 250 \text{ km s}^{-1}$, while for the remaining galaxies in our sample, the models show quiescent star formation with $T_* \leq 7 \cdot 10^4 \text{ K}$. A Seyfert 2 -like AGN is proposed in one galaxy. The O/H relative abundances derived by the detailed modelling of the spectra are nearly solar for all the sample galaxies, in contrast to those obtained by direct methods.

Key words. radiation mechanisms: general — shock waves — ISM: abundances — galaxies: Seyfert — galaxies: starburst — galaxies: high redshift

1. Introduction

In previous papers (Contini 2014, hereafter Paper I, Contini 2013, and references therein) we have investigated the physical conditions and element abundances in galaxies throughout redshifts $0.001 < z < 3.4$ by detailed modelling of the emission line ratios. We have found that both active galactic nuclei (AGN) and starbursts (SB) coexist in almost all galaxies and that collisional process should be accounted for.

In this paper we present modelling results of new spectra observed from selected galaxies at $1.4 < z < 3.5$ (Table 1), in particular those with enough lines (e.g. of oxygen in different ionization levels) that constrain the models (Paper I). We cross-check the models, when possible, by the upper limits of significant lines, by reproduction of the observed spectral energy distribution (SED) of the continuum, by the morphological evidence, etc.

We associate the ‘activity’ in galaxies (e.g. CDFS-695, van Dokkum et al 2005) to an AGN, a SB, and to shocks on the basis of a strong wind throughout the galaxy, while we refer to

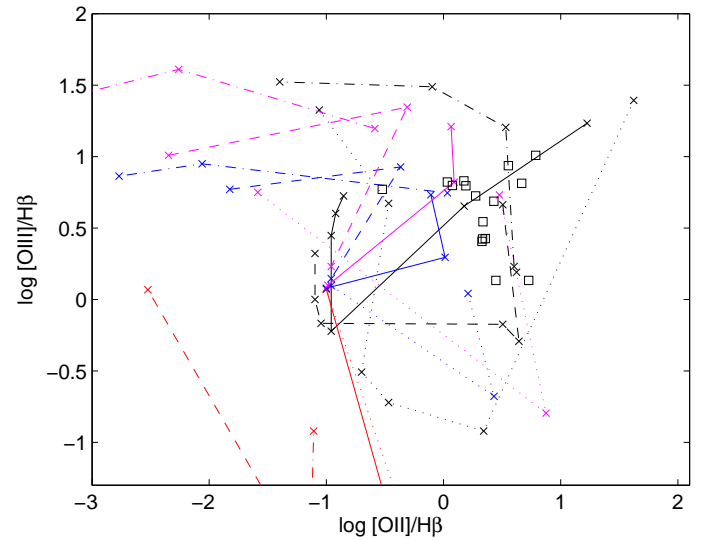


Fig. 1. Black open squares: the observation data. Black: AGN($V=100$ (dash-dot), 200 (dot), 300 (solid), 500 km s^{-1} (dash); $x: F=0, \log F=9, 10, 11, 11.5, 12$. SB: red ($T=10^4 \text{ K}$), blue ($T=5 \cdot 10^4 \text{ K}$), magenta ($T=10^5 \text{ K}$), $x: V=100, 300, 500 \text{ km s}^{-1}$, $U=0.01$ (dot), 0.1 (solid), 1 (dash), 10 (dot-dash)

Table 1. Description of the observed galaxies

object	z	galaxy type	telescope	ref
CDFS-695	2.225	luminous red	Gemini NIRS	1
1255-0	2.1865	quiescent	Gemini NIRS	2
A1835	2.073	low-mass SF	Hale tripelspec	3
A773	2.303	low-mass SF	Hale tripelspec	3
MACS0717	2.55	low-mass SF	Hale tripelspec	3
WISP	1.444-2.315	line selected	Mag. Baade (FIRE)	4
J1000+0221S	3.417	SF dwarf	CANDLES team	5

1: van Dokkum et al (2005); 2: Kriek et al (2006); 3: Belli et al (2013); 4: Masters et al (2014); 5: Amorín et al. (2014)

‘quiescent’ galaxies e.g. 1255-0, which was classified as a quiescent ultra-dense object by Kriek et al. (2009) because of emitting weak lines. Those imply a low luminosity AGN and a low star formation rate ($\text{SFR} = 1\text{--}3 \text{ M}_\odot \text{ yr}^{-1}$) compared with models of stellar population synthesis SEDs. In this paper we investi-

Table 2. Modelling the line ratios to $H\beta = 1$ observed by van Dokkum et al. (2005) and Kriek et al. (2009)

line	Obs ¹	M_{AGN}	M_{SB}	Obs ²	m_{AGN}	m_{SB}
z	2.225	-	-	2.1865	-	-
Ly α	-	41.87	53.97	-	30.39	27.7
NV 1240	-	0.007	0.072	-	0.31	1.27
CIV 1550	-	0.53	0.67	-	0.8	2.64
HeII 1640	-	3.43	3.32	-	0.89	0.16
[OII] 3727+	6.13	6.7	6.4	>5.33	6.	5.
[NeIII] 3869+	2.17	1.76	2.5	-	-	-
[OIII] 5007+	10.2	10	11.	<1.36	1.48	1.4
[OI] 6300+	<0.26	0.7	0.9	-	-	-
[NII] 6548+	2.46	3.2	3.6	>5.26	4.7	5.
H α	3.	3.	3.	3.07	3.	3.
[SII] 6718	0.5	0.5	0.29	>1.8	1.1	1.1
[SII] 6731	0.45	0.52	0.37	>0.67	1.1	1.7
$H\beta$ ³ _{qbs}	$2.9 \cdot 10^{-17}$	-	-	$<4.2 \cdot 10^{-18}$	-	-
$H\beta$ ³ _{mod}	-	0.059	0.051	-	0.013	0.009
V_s (km s ⁻¹)	-	100	250	-	180	150
n_0 (cm ⁻³)	-	150	130	-	100	300
F ³	-	40	-	-	1.6	-
T_* (10 ⁴ K)	-	-	20	-	-	-
U	-	-	0.03	-	-	0.007
D (10 ¹⁹ cm)	-	2	1	-	1.	0.6
N/H (10 ⁻⁴)	-	0.8	0.4	-	1.0	1.2
O/H (10 ⁻⁴)	-	6.6	5.6	-	5.6	6.6
S/H (10 ⁻⁴)	-	0.06	0.06	-	0.07	0.06

¹ van Dokkum et al. (2005); ² Kriek et al. (2009); ³ in erg cm⁻² s⁻¹; ⁴ in 10⁹ photons cm⁻² s⁻¹ eV⁻¹ at the Lyman limit

gate activity and quiescence in the galaxies described in Table 1, considering the SB effective temperature (T_*) and ionization parameter (U), the AGN flux intensity (F), and the shock velocity (V_s) as critical parameters.

In Sect. 2 we present calculations and modelling of the galaxy spectra. Results are presented and discussed in Sect. 3. Concluding remarks follow in Sect. 4.

2. The models

For the calculations of both the line and continuum spectra we adopted the code SUMA¹ (see also Contini et al. 2012), which accounts for the coupled effect of photoionization from a radiation source and shocks. The input parameters related with shocks are the shock velocity V_s , the atomic preshock density n_0 , and the preshock magnetic field B_0 . V_s determines the maximum temperature T of the gas downstream, near the shock front. The cooling rate in the recombination zone depends on the square density of the gas and on T in single slabs of gas. We adopt $B_0 = 10^{-4}$ Gauss.

The input parameter that represents the radiation field in AGNs is the power-law flux from the active centre F in number of photons cm⁻² s⁻¹ eV⁻¹ at the Lyman limit. The spectral indices are $\alpha_{UV} = -1.5$ and $\alpha_X = -0.7$. For SBs the radiation is a black body (bb). The input parameters are the effective temperature of the starburst T_* and the ionization parameter U (in number of photons per number of electrons at the nebula).

Additional input parameters are the geometrical thickness of the emitting nebula D which determines whether the model is radiation- or matter-bound, the abundances of He, C, N, O, Ne, Mg, Si, S, A, and Fe relative to H and the dust-to-gas (d/g) ratio which affect the cooling rate. The input parameters are all correlated throughout the Rankine-Hugoniot equations which regulate the shock dynamics at the shock-front and downstream,

and in the ionization equations that are used to calculate the ion fraction abundances for each element in each slab of gas downstream. Uncertainty in the calculation results is in average <10%.

The primary radiation flux and the secondary (diffuse) radiation flux, emitted by the gas slabs heated at relatively high temperatures by the shock, are calculated by radiative transfer throughout the clouds. The line ratios calculated by a power-law flux or by bb are different, so we calculate AGN and SB dominated models separately for all the galaxies. There is no degeneracy for the results of [OIII]/ $H\beta$ and [OII]/ $H\beta$ calculated by SB models as functions of T_* or of U , because the line intensities, which depend on the atomic configuration of the corresponding ions, show different trends with T_* and U .

Briefly, to reproduce the data by model calculations, we first choose the input parameter range from the grids of models (Fig. 1) calculated by Contini & Viegas (2001a,b, hereafter GRID1 and GRID2, for AGN and SB, respectively). Then we refine the fit (Tables 2-6) calculating new grids suitable to each spectrum. We cross-check the models resulting from the line spectrum fit by reproducing consistently the data in the continuum SED diagrams (Fig. 2), where for each model one line represents the bremsstrahlung (from the gas) and another, in the IR, the reprocessed radiation from dust. An initial grain radius of 0.2 μ m is adopted. The bb radiation fluxes from the SB and from the background old population stars also appear in Fig. 2 diagrams.

The results of detailed modelling are different from those obtained by direct methods because we calculate the emitted line fluxes integrating throughout the downstream recombination region where the shock determines the profile of electron temperature and density.

3. Results and discussion

3.1. The physical conditions and the element abundances

The set of input parameters which yields the best fit of calculated to observed data determines the model for each galaxy. It represents averaged conditions for each object when the observations cover the whole galaxy.

Generally, we have found that V_s , n_0 , and D result within the ranges calculated for a large number of objects (Paper I, Fig. 5), while the SB temperatures (Tables 2-3-5-6) $T_* = 2.5 \cdot 10^5$ K for CDFS-695 (van Dokkum et al) and A773 (Belli et al) are outstanding. $T_* \sim 7 \cdot 10^4$ K is found in the quiescent galaxy 1255-0 (Kriek et al), in WISP 170-106 (Masters et al.), and in A1835 (Belli et al.) and $T_* = 6.3 \cdot 10^4$ K in MCS 0717 (Belli et al.).

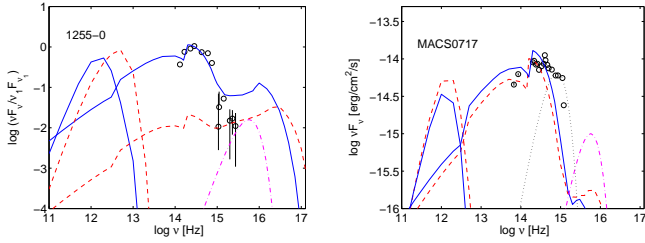
The results suggest that a strong starburst activity occurred in the two sample galaxies with maximum T_* , while quiescence is more adapted to the other galaxies with $T_* \leq 7 \cdot 10^4$ K similar to the starburst temperatures calculated for most of the objects in Paper I and in Contini (2013). $T_* = 2 \cdot 10^5$ K accompanied by a relatively high V_s in SBs is suitable to young stars and it may indicate a revival of activity in these galaxies. Such high temperatures were found, for example, in the recurrent nova T Pyxidis (Contini & Prialnik 1997), in the symbiotic star HM Sge at outburst (Angeloni et al. 2007), etc. The two ‘active’ galaxies also show a relatively high U (~ 1) and correspond to SFR ~ 60 and 400 M $_{\odot}$ yr⁻¹, respectively, which are derived from the H α luminosities (Kennicutt 1998).

The modelling presented in Tables 2, 3 and 6 suggests that AGN and SB coexist (see also Fig. 1) because the line ratios in each spectrum are satisfactorily fitted (within the observed errors) by both AGN and SB models. The same was found

¹ <http://wise-obs.tau.ac.il/~marcel/suma/index.htm>

Table 3. Modelling the line ratios to $H\beta = 1$ observed by Belli et al. (2013)

line	obs (A1835)	MB1 _{SB}	MB1 _{AGN}	obs(A773) ¹	MB2 _{SB}	MB2 _{AGN}	obs(MACS0717)	MB3 _{SB}	MB3 _{AGN}
z	2.073	-	-	2.303	-	-	2.55	-	-
[OII]3727+	2.17	2.3	2.2	4.65	4.6	4.8	2.27	2.2	2.3
[NeIII]3870	0.35	0.38	0.6	<4.3	1	0.85	< 1.07	0.29	0.5
[OIII]5007+	<3.5	3.45	3.47	6.5	6.4	6.7	2.67	2.8	2.6
H α	2.73	2.96	3.25	3.	3.6	3.4	2.9	2.96	3.16
[NII] 6384	0.33	0.386	0.39	0.59	0.47	0.6	0.7	0.57	0.59
$H\beta$ ²	$16.6 \pm 3.1 \cdot 10^{-17}$	-	-	$8.3 \pm 3.5 \cdot 10^{-17}$	-	-	$8.5 \pm 2.9 \cdot 10^{-17}$	-	-
$H\beta$ _{mod}	-	0.067	0.033	-	0.85	0.035	-	0.017	0.013
V_s (km s ⁻¹)	-	130	100	-	100	100	-	140	100
n_0 (cm ⁻³)	-	100	200	-	200	140	-	100	80
T_* (10 ⁴ K)	-	7	-	-	20	-	-	6.3	-
U	-	0.02	-	-	0.8	-	-	0.02	-
F^3	-	-	5.5	-	-	10	-	-	2
D (10 ¹⁹ cm)	-	1	1	-	6	1	-	1	1.5
N/H (10 ⁻⁴)	-	0.3	0.3	-	0.3	0.3	-	0.3	0.3
O/H (10 ⁻⁴)	-	6.6	5.5	-	7.6	6.6	-	6.6	5.6

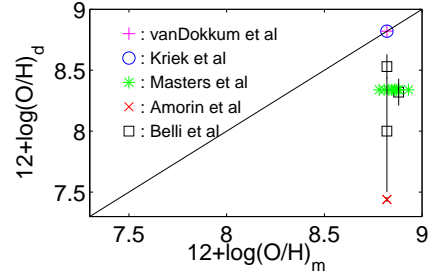
¹ reddening corrected; ² in erg cm⁻² s⁻¹; ³ in 10⁹ photons cm⁻² s⁻¹ eV⁻¹ at the Lyman limit

Fig. 2. SED of Kriek et al (2009, fig. 2) and Belli et al (2009, fig. 1) MACS0717 galaxies. Black circles : the data; blue solid lines : AGN models; red dashed lines : SB models; magenta dot-dashed lines : bb radiation calculated for T_* ; black dotted : bb for $T_* = 10^4$ K

throughout many local merger galaxies, due to mutual feed-backs. The AGN fluxes calculated for the present sample are similar to those found in low luminosity AGN (LLAGN), except for J1000+0221S (Amorín et al. 2014) which suits a Seyfert 2 galaxy.

We have found O/H close to solar ($6.6 \cdot 10^{-4}$, Allen 1976) for all the objects (Fig. 3). van Dokkum et al refer to diagnostic diagrams calculated by solar O/H and Kriek et al. mention solar or supersolar O/H. N/H modelled for Kriek et al. quiescent galaxy is similar to the maximum ($N/H = 1.4 \cdot 10^{-4}$) calculated in local galaxies (e.g. NGC 7212, Contini et al. 2012, fig. 14). Masters et al suggest an average $O/H = 2.18 \cdot 10^{-4}$ for their sample objects, while our models show O/H slightly higher than solar (Allen 1976), but within the solar $O/H = 8.5 \cdot 10^{-4}$ given by Anders & Grevesse (1989)(cf Paper I, table 1). Calculated N/H are generally lower than solar ($\sim 10^{-4}$), in agreement with the results obtained for galaxies in the same z range. For J1000+0.221S we found solar O/H and N/H, while Amorín et al. derived $O/H = 2.75^{2.88}_{2.6} \cdot 10^{-5}$ by the strong-line and calibration method presented by Maiolino et al. (2008) (see Paper I).

3.2. Notes on individual galaxies

CDFS-695. We cross-checked the results obtained by modelling the line spectrum (Table 2, col.3 and 4) calculating the distance r of the emitting cloud from the AGN in the NLR. The $H\beta$ flux observed at Earth ($2.9 \cdot 10^{-17}$ erg cm⁻² s⁻¹) after reddening correction (Osterbrock 1974, eq 7.6, fig. 7.1) results $H\beta_{obs} = 6.10^{-16}$


Fig. 3. Direct method (d) versus model (m) results for O/H

erg cm⁻² s⁻¹. Combining it with the $H\beta$ flux calculated at the cloud ($H\beta_{mod}$) : $H\beta_{obs} d^2 = H\beta_{mod} r^2$ (where d is the distance to Earth) and adopting a filling factor ~ 1 throughout the NLR, r results ~ 1.8 kpc, in rough agreement with van Dokkum et al who suggested the presence of shocks on the basis of the line ratios extending to ~ 10 kpc from the nucleus. The distance of the emitting clouds from the SB region, calculated in the same way, results $r < 1.9$ kpc, adopting a filling factor < 1 . The SB region does not cover the entire galaxy. SB have typical radii of 100-1000 pc (1-10% of the size of their 'host' galaxies).

1255-0. We constrained the models (Table 2) of this 'quiescent' galaxy (Kriek et al 2009) by the relatively low [OIII]5007+/[OII]3727+, [OII]/ $H\beta$, and [OIII]+/ $H\beta$ (Table 2, col. 5). The modelling results appear in Table 2, col. 6 and 7 (m_{AGN} , m_{SB}). The relatively low calculated $H\alpha$ flux ($\sim 3 H\beta_{mod}$) partly explains the low observed $H\alpha$ flux ($1.29^{+0.16}_{-0.18} \times 10^{-17}$ erg cm⁻² s⁻¹) and luminosity $L_{H\alpha}$ ($0.46^{+0.06}_{-0.06} \times 10^{-42}$ erg s⁻¹) confirming the low SFR observed by Kriek et al.

In Fig. 2 (left diagram) we model the continuum SED presented by Kriek et al. (2009, fig. 2). The data are normalized to unity at $1 \mu m$. The bremsstrahlung calculated by model m_{AGN} reproduces the data for ν between 10^{14} and 10^{15} Hz. The Planck function corresponding to $7 \cdot 10^4$ K peaks in the UV where the flux is strongly absorbed by the Galaxy. A few datapoints in the SED between 10^{15} and 10^{16} Hz fit the bremsstrahlung calculated by m_{SB} with perhaps some contribution from the bb flux from the SB. Models m_{AGN} and m_{SB} were calculated by dust-to-gas ratios (by number) of 10^{-15} and $10^{-14.3}$, respectively.

A1835, A773, and MACS0717. The results for the galaxies from the Belli et al. sample are presented in Table 3. Although the observed line ratios are typical of SBs, we have searched

Table 4. Modelling the line ratios ($H\beta = 1$) observed by Masters et al (2014)

WISP	z	[OII] 3727+	[OIII] 5007+	$H\alpha$	[NII] 6583	$H\beta_{obs}^1$
173-205	1.444	1.19	6.27	2.97	-	$7.5(0.4) 10^{-18}$
m1	-	1.1	6.3	3.03	0.19	-
9-73	1.454	1.88	5.3	4.	0.51	$31.6(1.3) 10^{-18}$
m2	-	2.0	5.4	3.2	0.40	-
25-53	1.486	2.13	2.55	2.8	0.51	$31.0(0.9) 10^{-18}$
m3	-	2.0	2.4	3.	0.42	-
46-75	1.504	2.8	1.36	3.05	0.45	$6.6(1.1) 10^{-18}$
m4	-	2.7	1.46	3.	0.37	-
170-106	2.165	3.57	8.64	4.	<0.35	$3.7(0.4) 10^{-18}$
m5	-	3.	8.32	2.9	0.13	-
64-210	2.177	1.49	6.76	4.2	0.75	$20.1(1.4) 10^{-18}$
m6	-	1.4	6.3	2.9	0.43	-
27-95	2.192	2.69	4.87	4.17	0.52	$18.6(0.7) 10^{-18}$
m7	-	2.67	4.57	3.1	0.4	-
90-58	2.212	2.15	2.65	3.79	0.54	$8.7(0.3) 10^{-18}$
m8	-	2.1	2.65	3.	0.5	-
56-210	2.304	1.55	6.25	2.8	-	$2.7(0.4) 10^{-18}$
m9	-	1.6	6.67	3.1	-	-
206-261	2.315	1.08	6.64	4.1	<0.15	$7.4(0.5) 10^{-18}$
m10	-	1.1	6.67	3.	0.13	-

¹ $H\beta$ observed flux in $\text{erg cm}^{-2} \text{s}^{-1}$. The uncertainty appears in parenthesis

Table 5. Gas physical conditions and relative abundances calculated for the Masters et al. (2014) sample

mod	V_s km s^{-1}	n_0 cm^{-3}	U -	T_* 10^4 K	D unit ¹	N/H 10^{-4}	O/H 10^{-4}	$H\beta_{mod}^2$ unit ²
m1	180	160	0.07	4.8	0.6	0.8	7.3	0.0036
m2	170	120	0.06	4.2	0.5	1.5	6.8	0.001
m3	140	150	0.03	4.0	1.0	0.7	7.	0.0046
m4	140	150	0.01	4.5	1.0	0.3	6.	0.0043
m5	320	200	0.12	7.5	3.0	0.1	8.5	0.1
m6	250	210	0.1	5.6	2.0	0.7	7.5	0.065
m7	230	100	0.05	4.	1.0	0.85	7.6	0.0013
m8	200	100	0.04	4.	2.0	0.8	6.4	0.0042
m9	180	160	0.07	4.5	0.4	0.8	7.3	0.0018
m10	180	160	0.07	4.8	0.6	0.6	7.6	0.0035

¹ 10^{16} cm ; ² $\text{erg cm}^{-2} \text{s}^{-1}$;

for AGNs in each object. The results show that AGN could be present (Fig. 1). T_* is relatively high, in particular for A773 ($2 \cdot 10^5 \text{ K}$). The emitting clouds are geometrically thick ($D \geq 10^{19} \text{ cm}$) which seems unusual for AGNs in this z range ($D \leq 10^{16} \text{ cm}$, Contini 2013, fig. 3). The models selected for MACS0717 (Table 3) are cross-checked by fitting the SED in Fig. 2. The observed photometry follows the bremsstrahlung maximum. The peak frequency depends on V_s and the peak intensity on F . The old star background population contributes to the MACS0717 SED by a bb flux corresponding to a temperature of 10^4 K .

The WISP galaxies. The modelling of line ratios from the Masters et al sample of galaxies (Table 1) with prominent $H\alpha$ and/or [OIII] lines, is shown in Table 4. We selected the galaxies corresponding to $2.8 < H\alpha/H\beta < 4.2$, i.e. those which do not need reddening correction (Osterbrock 1974). Modelling results appear in Table 5. WISP 170-106 shows a relatively high shock velocity (320 km s^{-1}) and a relatively high U (0.12) for $T_* = 7.5 \cdot 10^4 \text{ K}$ suggesting a fading activity.

J1000+0221S. Amorín et al. (2014) report the spectrum observed from this strongly gravitationally lensed galaxy. The observed line ratios appear in Table 6. They are similar to those calculated by models presented in GRID1 (table 4, mod 36) for AGNs and in GRID2 (table 1, mod 6 and table 2, mod 7) for SBs. The AGN flux $F = 3 \cdot 10^{11} \text{ photons cm}^{-2} \text{s}^{-1} \text{ eV}^{-1}$ at the Lyman

Table 6. Comparison of model results with the data for J1000+0221S (Amorín et al. 2014)

	obs	M_{AGN}	$M1_{SB}$	$M2_{SB}$
z	3.417	-	-	-
[OII]3727	<0.3	0.3	<0.5	0.43
[NeIII]3869	<0.2	0.2	0.25	0.4
[OIII]5007+4959	5.9 ± 2.6	4.7	5.5	8.45
$H\beta$	1	1	1	1
$H\beta_{mod}^1$	-	21.9	0.13	2.58
$V_s (\text{km s}^{-1})$	-	200	100	200
$n_0 (\text{cm}^{-3})$	-	200	100	200
F^2	-	3	-	-
$T_* (10^4 \text{ K})$	-	-	5	5
U	-	-	0.1	1
$D (10^{19} \text{ cm})$	-	1	1	1
O/H (10^{-4})	-	6.6	6.6	6.6
N/H (10^{-4})	-	0.9	0.9	0.9

¹ in $\text{erg cm}^{-2} \text{s}^{-1}$; ² in $10^{11} \text{ photons cm}^{-2} \text{s}^{-1} \text{ eV}^{-1}$ at the Lyman limit

limit, is suitable to Seyfert 2 AGN and is higher by ~ 7 -200 than in the other galaxies of the present sample. Amorín et al. define this object as a metal-poor star forming galaxy based on the low O/H and low U deduced by empirical +photoionization method. Our models show different results because of the coupled effect of photoionization and shocks. This would lead to a different mass-metallicity- SFR relation.

4. Concluding remarks

The high starburst temperature ($T_* \sim 2 \cdot 10^5 \text{ K}$) suggesting activity in the two galaxies CDFS-695 (van Dokkum et al. 2005) and A773 (Belli et al 2013) is not seen in the other galaxies of the modelled samples. Activity in terms of a Seyfert 2 AGN flux is found in the J1000+0221S galaxy (Amorín et al 2014). The ionization parameter U calculated for the galaxy bulk shows larger scattering than F because U depends on the hot source radiation flux as well as on the ISM conditions. So it is less significant to activity than F which depends mainly on the intensity of the non-thermal radiation flux from the AGN.

By detailed modelling of the spectra we have found O/H close to solar (Allen 1976, Anders & Grevesse 1989). N/H are generally lower than solar, in agreement with the results obtained for galaxies at those redshifts.

Acknowledgements

I am grateful to the referee for useful comments.

References

- Allen, C.W. 1976 Astrophysical Quantities, London: Athlone (3rd edition)
- Amorín, R. et al. 2014, ApJL, 788, L4
- Anders E., Grevesse N. 1989, Geochim. Cosmochim. Acta, 53, 197
- Angeloni, R., Contini, M., Ciroi, S., Rafanelli, P. 2007, AJ, 134, 205
- Belli, S., Jones, T., Ellis, R.S., Richard, J. 2013 ApJ, 772, 141
- Contini, M. 2014, A&A, 564, 19, Paper I
- Contini, M. 2013, arXiv1310.5447
- Contini, M., Cracco, V., Ciroi, S., La Mura, G. 2012, A&A, 545, 72
- Contini, M. & Prialnik, D. 1997, ApJ, 475, 803
- Contini, M. & Viegas, S.M.A. 2001a, ApJS, 132, 211, GRID1
- Contini, M. & Viegas, S.M.A. 2001b, ApJS, 137, 75, GRID2
- Kennicutt, R.C. 1998, ARA&A, 36, 189
- Kriek, M., van Dokkum, P.G., Labbe', I., Franx, M., Illingworth, G.D., Marchesini, D., Quadri, R.F. 2009, ApJ, 700, 221
- Kriek, M. et al. 2006, ApJ, 649, L71
- Maiolino, R. et al. 2008, A&A, 488, 463

M. Contini: Activity and quiescence in galaxies at redshifts $1.4 < z < 3.5$. The role of the starburst temperature. (*RN*)

Masters, D. et al. 2014, ApJ, 785, 153

Osterbrock, D.E. 1974 in Astrophysics of Gaseous Nebulae. W.H.Freeman and Company, San Francisco, Ed.

van Dokkum, P.G., Kriek, M., Rodgers, B., Franx, M., Puxley, P. 2005, ApJ, 622, L16